

## Effect of Backing Board on the Heat Release Rate of Wood

Mark Dietenberger  
U.S. Department of Agriculture, Forest Service,  
Forest Products Laboratory<sup>1</sup>  
Madison, Wisconsin

**Abstract.** Cone calorimeter tests of wood with three different backings showed that the backing did not affect time to ignition, initial peak heat release rate (HRR), and total heat release, at four different imposed heat fluxes. However, use of dense backing board for the Steiner tunnel test eliminated the second peak in the HRR profile and prolonged the intervening period of simultaneous flaming and glowing combustion, as evidenced by a gradual increase in the heat of combustion with time. Gypsum backing board had an intermediate effect on the HRR profile. The volatile and glowing effective heats of combustion were separately invariant with time for at least two wood specimens, southern yellow pine and redwood, regardless of the backing and imposed heat flux. This observation was used to reconstruct separate HRR profiles (and mass loss rate) for flaming and glowing. An analytical thermal wave solution for the temperature profile was fitted to thermocouple data for exposed and protected sides of southern yellow pine, resulting in reasonable thermal properties. The char front position, as identified with char temperature on the thermal wave profile, was converted to flame heat release (FHR) by multiplying it with the volatile heat of combustion, the mass fraction of volatile gases, the initial specimen mass, and the inverse of specimen thickness. Differentiation of FHR resulted in a flame HRR somewhat in agreement with the post-peak decreasing HRR data. Predicted thermal wave depth reached specimen thickness (25.3 mm) at 230 s, at which point (1) temperatures began to rise for the protected side of the specimen, (2) HRR data started to level out, and (3) HRR profiles began to diverge as a result of backing board variations. These results will influence testing protocols for cone calorimeter and modeling techniques for fire growth.

### Introduction

Our recent study on mathematical modeling and the standard room burn test (ISO9705) and flame spread test (Steiner tunnel test, ASTM E84) raised a question about whether the specimen backing used in these large tests should be used in cone calorimeter tests (ASTM E1354). Initially, we used only insulation backing for cone calorimeter test specimens. The test specimens were identical to those used in large-large tests. Preliminary tests on oriented strandboard (OSB) with three different backings showed that the backing affected the overall HRR profile. Therefore, we conducted cone

---

<sup>1</sup> The Forest Products Laboratory is maintained in cooperation with the University of Wisconsin. This article was written and prepared by U.S. Government employees on official time, and it is therefore in the public domain and not subject to copyright.

calorimeter tests of some room burn specimens using gypsum and dense board as backing at flux levels of 20, 35, 50, and 65 kW/m<sup>2</sup>. This paper presents results for southern yellow pine and redwood specimens.

Our results thus far indicate that although specimen backing does not affect time to ignition, peak HRR, and THR, it nevertheless significantly reduces the typical second peak HRR. This seems to add credence to using exponentially decreasing functions for HRR profiles. On the other hand, backing board has been known to affect fire performance in some full-scale fire tests, which would favor the flat profile for HRR, at least by providing a sensitivity to the effects of backing board. A factor to consider is the high sensitivity of analytical fire growth models (those that use exponentially decreasing HRR) on the accuracy of initial peak HRR and the derived ignition temperature. For example, in our recently developed analytical flame spread model for the Steiner tunnel, a 10% difference in measuring the peak HRR for Douglas-fir plywood would produce a 27% difference in the flame spread index (FSI = 91.2 for plywood). Recent round robins with the cone calorimeter indicate at least a 10% error in peak HRR for the 95% confidence level. In addition, the experimental decrease with respect to time in post-peak HRR is usually more rapid than the fitted exponential decreasing function. Finally, there is the question of how much of the HRR profile is affected by backing board.

Guidance on the influence of the backing board is scant in existing literature. Related to the HRR profile are many publications on investigations of wood pyrolysis and charring. Detailed mechanistic pyrolysis models that include chemical kinetics (Bryden 1998, Parker 1988; models and literature review) provide insight to the pyrolysis process, but typically do not consider backing materials. One exception is Ritchie et al. (1997), who claim that according to model predictions the second peak HRR is very sensitive to the thickness of the insulating substrate, although no specific results or figures are given. At this time, however, intensive computations of these models prevent their use in fire growth models. To address the computation problem, some researchers have reduced pyrolysis modeling to a Stefan problem (Jia et al. 1999, Moghtaderi et al. 1997a) that uses heat of pyrolysis and a very thin zone of charring at constant temperature. Again, predictions including backing board were not available.

The experimental and modeling results of Staggs and Whitely (1999), who studied ablative pyrolysis of 10-mm-thick plastic on a circular bulky ceramic holder, are relevant to our study. These authors established the superiority of thermal degradation kinetics in mechanistic models to that of Stefan problems in modeling initial rise in mass loss rate (MLR) to a steady value. Since the measured heat of pyrolysis decreases with char mass fraction and can even become negative for wood (Bryden 1998), the heat of pyrolysis derived in Stefan problems to predict initial rise in MLR to a peak value can be largely fictitious. Secondly, when Staggs and Whitely increased the density of the ceramic sample holder, the modeled peak MLR near burnout time decreased in value while the MLR profile in the first 200 s of the test remained unaffected. As reported later in this paper, we also found this effect with the MLR of wood when a backing board was used.

The results of Staggs and Whitely show a very sharp drop in MLR after the peak, which is typical for non-charring materials. In the case of wood, MLR drops gradually after the second peak, mainly because of glowing combustion (char oxidation). Data by Moghtaderi et al. (1997b) indicate a fairly sharp transition from flaming to glowing after the second MLR peak, as evidenced by an increase in effective heat of combustion (EHC) and change in specimen color from black to red. When plotted as a function of time, EHC was relatively constant during flaming and glowing at five incident heat fluxes. Our work also confirmed this effect, with the exception that the transition from flaming to glowing was much more gradual, particularly when a backing board was used.

This paper also includes a reconstruction of the volatile and glowing HRR (and MLR) profiles based on the idea that flaming and glowing at a location are mutually exclusive, but side by side in the case of flames emitting from char fissures. Finally, a thermal wave model is developed to provide a direct link between the decreasing charring rate and the decreasing flaming HRR during the thermal wave phase.

### **Effect of Backing on Southern Yellow Pine and Redwood Summary Data**

The matrix of test data and test methods was as follows. For each conditioned (50% relative humidity (RH) at room temperature) southern yellow pine and redwood sample and flux level, two tests were conducted with no backing board, one test with 12.5-mm-thick gypsum board (from ISO 9705 as one of five alternatives), and one test with 6.25-mm-thick inorganic reinforced cement board (from ASTM E84). Aluminum foil was wrapped around the wood-backing board specimen, which was then laid on a layer of low-density refractory fiber blanket in a horizontal specimen holder and covered with a retainer frame. When it became apparent that thermocouple measurements were necessary (after three-quarter of the tests were completed), three thermocouples (0.25-mm beads) were attached by (1) embedding one (using a razor blade) into the center of the exposed surface, (2) cementing one to the cement board and pressing it against the protected side of the specimen, and (3) cementing the third to the cold side of the cement board. Specimens were exposed to heat fluxes of 20, 35, 50, and 65 kW/m<sup>2</sup>.

Figures 1 and 2 provide results on time to ignition, peak HRR, and THR as a function of imposed heat flux for southern yellow pine and redwood, respectively. For each heat flux level for each parameter, four data points are associated with variations of backing conditions. These results were not detectably influenced by the backing material, so we do not identify the data points pertinent to the different backing materials. Intuitively, the backing condition should affect neither the time to ignition nor the peak HRR, as verified in these tests. The lack of observed systematic variations of THR with backing condition indicates that a decreasing value of the second peak HRR with the denser backing is compensated by a longer burnout time to achieve an unchanging THR. The high random variations in all parameters for both wood samples at 20 kW/m<sup>2</sup> is consistent with that described in the ISO 5660 document for materials tested close to the critical fluxes of ignition. However, parameters for redwood were much less random than those for southern yellow pine at the higher fluxes of 35, 50, and 65 kW/m<sup>2</sup>. The random errors in

time to ignition and THR for redwood were clearly less than 10% whereas those of peak HRR remained significantly above 10%. Overall, peak HRR and THR increased linearly with heat flux and time to ignition had the expected inverse power function relationship with heat flux.

### **Effect of Backing on HRR Profile at 35- and 50-kW/m<sup>2</sup> Fluxes**

The HRR profiles for southern yellow pine (Figs. 3 and 4) and redwood (Figs. 5 and 6) at 35- and 50-kW/m<sup>2</sup> fluxes are consistent with the results of Staggs and Whitely (1999) for their MLR profile: a denser backing reduced the second peak HRR and the initial (first 200 to 400 s) HRR profile remained basically unchanged. Specifically, the cement backing could eliminate the second peak HRR, whereas the gypsum backing was not as effective and varied with flux level. The corresponding MLR data for southern yellow pine and redwood have the same qualitative features as those of the HRR profiles (data not shown). Similar results were achieved at 20- and 65-kW/m<sup>2</sup> fluxes and with other wood products tested at the Forest Products Laboratory (data not shown). With respect to the Staggs and Whitely data for plastic, the differences for wood are the appearance of the initial peak MLR from charring and a gradual drop in MLR after the second peak HRR from glowing.

### **Reconstruction of Flame and Glow HRR Profile for Southern Yellow Pine**

It has become clear, particularly with regard to specimen backing, that HRR as computed in the standard (ASTM E1354) needs to be corrected for experimental bias to be useful in fire growth models. Although several researchers have shown a demarcation of EHC into an initial heat of combustion from volatile gases followed by glowing, we offer here a finer analysis of EHC not previously considered. Because HRR is affected by the time delays and responses of the oxygen consumption method, it is not synchronized with MLR. Therefore, the EHC, computed as HRR divided by MLR, has a systematic bias. An obvious correction is to perform a time shift and a deconvolution of time response of HRR to create a reconstructed HRR that is synchronized with MLR. Various methods of deconvolution cause the noise of reconstructed HRR to be about as great as the HRR values themselves. The high MLR noise level also compounds the problem of computing EHC. However, the raw data for specimen mass appear as a smoothly decreasing function of time (see Fig. 7) and the MLR is dependent on the differentiation formula prescribed in the standard. Thus, a trapezoidal numerical integration of the reconstructed HRR (the selected deconvolution is described in Diertenberger 1996) provides a relatively smooth THR profile, as shown in Figure 7. This THR is then in synchronization with the mass loss (MLS), the specimen mass at ignition minus its current mass. The identical differentiation formula, using Savitsky–Golay coefficients derived from least-squares parabolas sliding on a window size of five points, is applied to “reconstructed” THR and MLS to obtain a low-noise and low-bias EHC (Fig. 7). The result is a heat of combustion that is more of a constant during flaming and more of a gradual rise during transition from flame to glow as compared to the standard computations.

The next step in the HRR reconstruction is to separate THR into flame and glow components as

$$\text{THR} = \text{FHR} + \text{GHR} = \text{EHC}_{\text{flame}} (\text{MLS} - \text{MLG}) + \text{EHC}_{\text{glow}} \text{MLG} \quad (1)$$

During the initial period, the mass loss of glowing (MLG) is zero, which allows calculation of a value for effective heat of combustion of volatile gas. Likewise, near the end of the test the flaming ceases and FHR reaches a maximum value, which allows calculation of a value of effective heat of combustion for glow. These values for heat of combustion are substituted into Equation (1) so that MLG is calculated as a function of time and increases monotonically. In this way, the flaming heat release and glowing heat release are also obtained as a function of time. Other combustion parameters can be derived more accurately, such as the mass fractions converted to volatile gases and char:

$$f_{\text{char}} = 1 - f_{\text{vol}} = (M_{\text{end}} + \text{MLG}_{\text{end}}) / M_{\text{start}} \quad (2)$$

This leads to computing the net char mass production as function of time

$$M_{\text{char}} = f_{\text{char}} (\text{MLS} - \text{MLG}) / f_{\text{vol}} - \text{MLG} \quad (3)$$

which is shown in Figure 7 as gradually increasing with time and then decreasing with time as the glowing mass loss begins to dominate. The flaming and glowing HRR profile is conveniently obtained with another form of Equation (1) by differentiating it with time to obtain

$$\text{HRR} = \text{EHC} \text{MLR} = \text{EHC}_{\text{flame}} \text{MLR} + (\text{EHC}_{\text{glow}} - \text{EHC}_{\text{flame}}) \text{MLR}_{\text{glow}} \quad (4)$$

Solving for the MLR of glowing and multiplying by heat of combustion of glow results in

$$\text{HRR}_{\text{glow}} = \text{EHC}_{\text{glow}} \text{MLR} (\text{EHC} - \text{EHC}_{\text{flame}}) / (\text{EHC}_{\text{glow}} - \text{EHC}_{\text{flame}}) \quad (5)$$

which is the heat release rate of glowing. The heat release rate of flaming is given by the heat of combustion of flaming multiplied by the mass loss rate of volatile gases:

$$\text{HRR}_{\text{flame}} = \text{EHC}_{\text{flame}} (\text{MLR} - \text{MLR}_{\text{glow}}) \quad (6)$$

Figure 8 shows the result of reconstructing the HRR profiles specifically for southern yellow pine exposed to 50 kW/m<sup>2</sup> and backed by cement board. The “HRR data” profile in Figure 8 is identical to the fourth HRR profile in Figure 4; the next three HRR profiles were computed with Equations (4), (5), and (6), respectively. Note that if HRR from Equation (4) is shifted in time by 16 s and filtered with a time constant of 9.3 s, it would be in closer agreement with the HRR data profile, particularly around the initial peak HRR. Of significance is the appearance of glowing combustion at about 700 s, which is less than half the burn time and 300 s less than the time of the second peak HRR. The period of simultaneous flaming and glowing is about 700 s. This result demonstrates the importance of correcting for the bias in the EHC profile and accounting for the effect of backing conditions during simultaneous flaming and glowing. The significance of Equation (6) is that it provides the flaming HRR profile applicable to fire growth scenarios that include large burner flames covering the charred surfaces, which should prevent glowing combustion by vitiating surface oxygen.

## Thermal Wave Solution for Southern Yellow Pine Flaming HRR Profile

For the case of instant exposure to imposed radiant heat flux with convective/re-radiation cooling, our finite element solutions show a nearly cubical temperature profile that initially travels as a thermal wave from the surface through the material without any influence from the specimen thickness. For the duration of the thermal wave, the specimen backside temperature remains at the initial temperature and the backing conditions cannot have any effect on the heating processes within the specimen. The thermal wave takes on a different form once the backside temperature begins to increase and the backing material has a thermal diffusivity different from that of the test material. Another change to the thermal wave occurs at surface ignition: the flame adds a surface heat flux greater than  $10 \text{ kW/m}^2$ , sending a second thermal wave into the specimen. Even if the imposed surface heat flux does not change (e.g., flux from the ignition burner), significant surface charring will produce changes to surface emissivity and thermal conductivity that in effect will send the second thermal wave into the specimen. The cubical temperature profile in the second thermal wave is also a very good approximation providing that (1) the heat of pyrolysis is negligible, (2) the thermal diffusivity values of char and wood are similar, and (3) for conditions of significant char contraction, the char depth is small compared to thermal wave depth. For some wood specimens, these assumptions of thermal properties are valid (see Parker 1988).

In this paper we consider the temperature slightly above that of ignition to define the char front depth within the simultaneous first and second thermal waves. As will be derived, this results in an analytical prediction of char depth as a function of time. The differentiation of the char depth solution with time is easily computed and converted to flaming HRR in the following calculations. The thermal wave is the solution of the following thermal diffusion and boundary condition equations at the exposed surface:

$$\partial(T - T_a)/\partial(\alpha t / \delta_m^2) = \partial^2(T - T_a)/\partial X^2 \quad (7)$$

$$\partial(T_s - T_a)/\partial X = (h_s \delta_m / \lambda_m)(T_s - T_a) - (\epsilon_s q_s \delta_m / \lambda_m) \quad (8)$$

Although exact solutions involving error functions are available, the intent here is to provide a good approximation that results in an analytic formula suitable for use in least-squares regression routines. For approximated solution, the cubic temperature profile is the power function

$$(T - T_0) = (T_s - T_0)(1 - X \delta_m / \delta)^3 \quad (9)$$

where surface temperature  $T_s$  and thermal wave depth  $\delta$  are functions of time. Substituting Equation (9) into Equations (7) and (8) and solving, the exact formula is

$$B - \ln(1 + B) = 6F_m B_m^2 \quad (10)$$

$$T_s - T_a = [(T_0 - T_a) + (\epsilon_s q_s / h_s)B] / (1 + B) \quad (11)$$

$$B = h_s \delta / 3 \lambda_m \quad (12)$$

$$F = \alpha / \delta^2 \quad (13)$$

The subscript  $m$  for  $B$  and  $F$  means substitution of thermal thickness by material thickness. The thermal wave depth is given by the implicit formula, Equation (10). It can be made explicit by approximating the left side of Equation (10) to the first order by the term  $B^2 / (B + 2)$ . Its greatest error is  $-10\%$  at  $B = 2$  and approaches exact value as  $B$  approaches zero or infinity. With this substitution, we have approximately

$$B \approx 3F_m B_m^2 + \sqrt{(3F_m B_m^2)^2 + 12F_m B_m^2} \quad (14)$$

A noteworthy aspect is the absence of imposed flux and temperature in Equation (10) as factors influencing the thermal depth. A maximum value allowed for the Fourier number  $F_m$  (and thus also the critical test time) for validity of the thermal wave solution is solved by Equation (10) with the thermal depth set equal to the specimen thickness. If the cooling heat transfer coefficient is also negligible in Equation (10), the maximum Fourier number is equal to  $1/12$ . This means that 19-mm-thick southern yellow pine with a derived thermal diffusivity of  $0.16 \text{ mm}^2/\text{s}$  (Dietenberger 1999) corresponds to the critical test time of 190 s, beyond which the backing conditions begin to affect the charring rate and the HRR profile. A finite value of the cooling heat transfer coefficient would somewhat decrease the critical test time, as will be shown later. The composite thermal wave entering the specimen upon ignition is solved with the supposition of first and second thermal waves. The char position corresponds to the charring temperature value on the composite temperature profile, as in

$$T_{\text{ch}} - T_0 = (T_{\text{s1}}(t) - T_0) \left(1 - \frac{X_{\text{ch}} \delta_m}{\delta_1(t)}\right)^3 + \left[ T_{\text{s2}}(t - t_{\text{ig}}) - T_{\text{s1}}(t - t_{\text{ig}}) \right] \left(1 - \frac{X_{\text{ch}} \delta_m}{\delta_2(t - t_{\text{ig}})}\right)^3 \quad (15)$$

At a constant char temperature, Equation (17) is a cubic function of the charring position and is solved analytically by standard algorithms. Charring position is converted to flame heat release by the formula

$$\text{THR}_{\text{flame}} = \text{EHC}_{\text{flame}} f_{\text{vol}} M_{\text{start}} X_{\text{ch}} \quad (16)$$

that when differentiated with respect to time gives the flame HRR. Examination of Equations (10) to (13) indicates the need to obtain the values for (a) imposed heat flux to cooling heat transfer coefficient ratio, (b) cooling heat transfer coefficient to material thermal conductivity ratio, and (c) material thermal diffusivity for both thermal waves for application in Equations (15) and (16). For this purpose, we embedded a 0.25-mm thermocouple bead into the exposed surface, using a razor blade, and pinned the thermocouple wires onto the sample holder to avoid weight loss errors. During testing, we recorded the temperature profile using the cone calorimeter software and a thermocouple signal converter. The data typically showed a rapid increase in temperature upon exposure to imposed flux and also at the point of ignition (Fig. 9). Although in most cases the thermocouple remained attached after charring, it eventually developed a noise level associated with flame flickering. Figure 9 shows the fit of Equation (17) to the data from the embedded thermocouple. We used an optimum thermocouple depth of 0.13 mm for the term  $X_{\text{ch}} \delta_m$ . Using an emissionmeter to measure long wavelength emissivity, we obtained a surface emissivity of 0.88. A convective cooling coefficient of  $0.021 \text{ kW/m}^2 \text{ K}$  for a cone heater flux of  $50 \text{ kW/m}^2$  (Dietenberger and Grexa 1999) was also obtained. Using the following formula for the cooling heat transfer coefficient prior to ignition,

$$h_s = h_c + \epsilon\sigma(T_{ig}^2 + T_a^2)(T_{ig} + T_a) \quad (17)$$

the ignition temperature and material thermal conductivity were derived as 557 K and  $2.54 \times 10^{-4}$  kW/m K, respectively (recall that thermal diffusivity is  $0.16 \text{ mm}^2/\text{s}$ ) as a fit to the Figure 9 data. For the time after ignition, the flame imposes a convective and radiative heat flux of undetermined amount. The cooling heat transfer coefficient as given by Equation (17) is then modified by setting the convective component to zero and substituting the ignition temperature by the equilibrium temperature (Equation (8) is set to zero to solve for equilibrium temperature). It is through Equation (17) that imposed flux and temperatures will affect the critical test time as evaluated with  $B = B_m$  in Equation (10). During charring, the emissivity is set to unity and the imposed heat flux and char thermal conductivity are then derived as  $63.6 \text{ kW/m}^2$  and  $2.55 \times 10^{-4}$  kW/m K, respectively, as a fit to Figure 9 data. This gives a reasonable flame heat flux of  $13.6 \text{ kW/m}^2$  as well as reasonable thermal properties of wood and char. The charring temperature of 330 C (603 K) provides the optimum fit of Equation (16) to the FHR data shown in Figure 7.

Figure 8 provides details for comparing the differentiation of Equation (16), described as the thermal wave solution, with the HRR data. The thermal wave solution has a very sharp initial HRR peak and then continuously decreases until a sharp drop appears at 1170 s as a result of the arrival of the charring temperature (300 C) at the wood thickness. Selecting a charring temperature of 350 C provides a better agreement with the HRR data for the first 230 s and provides a HRR cutoff at around 1,400 s. The use of degradation kinetics in mechanistic models should provide agreement with the peak HRR and with a gradual decrease in flaming HRR during a second peak HRR. The cement-backed 6.25-mm-thick board seemed quite effective in lowering the flaming HRR almost to the level predicted by the thermal wave solution. Thus, the board appears to allow the thermal wave to pass through undiminished. Using a total specimen thickness of 25.25 mm (wood and board) in Equation (10) with  $B = B_m$ , the test time in which the insulation backing will begin to affect the HRR is 230 s. Without the backing, the critical test time with a cooling heat transfer coefficient of  $0.038 \text{ kW/m}^2 \text{ K}$  is 130 s. These critical test times are consistent with the rise in temperature of the cement board (Fig. 9) and with diverging HRR profiles resulting from various backing conditions (Figs. 3 to 6).

## Conclusions

Our observations of the HRR profile derived for wood affect the protocols for cone calorimeter testing and the material properties for input to fire growth modeling:

1. Redwood had less than 10% error in time to ignition and THR while corresponding errors for southern yellow pine greatly exceeded 10% over the four incident fluxes tested. However, despite being a more consistent material to test, redwood still had large errors in the peak HRR that could be related to the inability of the cone calorimeter to effectively capture the sharp HRR peak or to variable degradation kinetics of the wood surface. A fire growth model based on the exponentially

decreasing function of HRR is quite sensitive to the value of peak HRR, which means that such an analytic profile should be fitted to the post-peak HRR profile rather than the peak HRR.

2. No consistent effect of backing, whether insulation, gypsum board, or dense E84 board, could be identified for the time to ignition, initial peak HRR, or THR. Therefore, in cases where a backing material affects a fire performance result of a large test, these summary parameters of the cone calorimeter should not be used as the sole basis for correlating or modeling with large-scale tests.
3. The cement backing eliminated the second HRR peak and stretched out the period of simultaneous flaming and glowing. The gypsum backing had an intermediate effect. These results necessitated a reconstruction of separate HRR profiles for volatiles and char for use in fire growth models that simulate the use of a large pilot burner, which would prevent glowing on charred surfaces. One result was a better determination of the fraction of material converted to volatile gases and of the constancy for the effective heat of combustion for the volatile gases.
4. A thermal wave model was used to predict that backing conditions cannot affect the HRR profile during the first 190 s of any test for 19-mm-thick southern yellow pine. Variations in cooling heat transfer coefficient or backing thermal properties affect the critical test time to some extent, whereas the values of imposed heat fluxes or charring temperatures only indirectly affect the critical test time through their effects on the cooling heat transfer coefficient.
5. If a particular charring condition results in a negligible heat of pyrolysis, then our results with a thermal wave solution for the flaming HRR show a need for a mechanistic model that incorporates degradation kinetics to predict the peak HRR and the gradual decrease in flaming HRR near the burnout time. Indeed our results with two different charring temperatures (300 and 350 C) can be qualitatively used to demonstrate the inherent deficiency of using Stefan-type modeling that relies on a constant charring temperature for calculating the total HRR profile.

The thermal diffusivity values of 12.5-mm-thick gypsum board used in room tests (ISO9705) are similar to those of wood. When this gypsum board is used in combination with 19-mm-thick southern yellow pine, 510 s of testing occur before the room's 20-mm thick calcium silicate back wall begins to affect the HRR profile. Worse yet, when 6.25-mm-thick, dense E84 board (which has somewhat higher thermal diffusivity than that of gypsum board) is used in combination with southern yellow pine, 330 s of testing occur before the 50-mm-thick mineral composition insulation in the Steiner tunnel board begins to affect the HRR profile. These critical test times assume negligible values of cooling heat transfer coefficient, which, if finite, will further decrease the critical test times. Since the burnout time for southern yellow pine is approximately 20 min, another round of cone calorimeter tests should be done to include the secondary backing material for a total thickness of 50 mm.

## References

- Bryden, K.M., 1998, Computational modeling of wood combustion, Ph.D. dissertation, Mechanical Engineering Department, University of Wisconsin, Madison, Wisconsin.
- Dietenberger, M.A. and Grexa, O., 1999, Analytical model of flame spread in full-scale room/corner tests (ISO9705), In Proceedings of Fire and Materials '99, Feb. 22–23, 1999, San Antonio, Texas.
- Dietenberger, M.A., Grexa, O., White, R.H., Sweet, M., and Janssens, M., 1995, Room/corner tests of wall linings with 100/300 kW burner, In Proceedings of 4<sup>th</sup> Fire and Materials Conference, London. Interscience Communications: 53–62.
- Jia, F., Galea, E.R., and Patel, M.K., 1999, Numerical simulation of the mass loss process in pyrolyzing char materials, *Fire and Materials*, 23: 71–78.
- Moghtaderi, B., Novozhilov, V., Fletcher, D.F., and Kent, J.H., 1997a, An integral model for the transient pyrolysis of solid materials, *Fire and Materials*, 21: 7–16.
- Moghtaderi, B., Novozhilov, V., Fletcher, D.F., and Kent, J.H., 1997b, The effect of char oxidation on the flaming combustion characteristics of wood materials, *Journal of Applied Fire Science*, 6(3): 189–201.
- Parker, W.J., 1988, Prediction of the heat release rate of wood, Ph.D. dissertation, Mechanical Engineering Department, George Washington University, Washington, D.C.
- Ritchie, S.J., Steckler, D.S., Hamins A., Cleary, T.G., Yang, J.C., and Kashiwagi, T., 1997, The effect of sample size on the heat release rate of charring materials, In Proceedings of 5<sup>th</sup> International Symposium, Fire Safety Science, 177–188.
- Staggs, J.E.J. and Whitely, R.H., 1999, Modeling the combustion of solid-phase fuels in cone calorimeter experiments, *Fire and Materials*, 23: 63–69.

## Nomenclature

$B$	Dimensionless thermal thickness (Eq. 12)	THR	Total heat release (MJ/m <sup>2</sup> )
EHC	Effective heat of combustion (MJ/kg)	$X$	Depth relative to material thickness (–)
$f$	Mass fraction	$\alpha$	Thermal diffusivity (m <sup>2</sup> /s)
$F$	Dimensionless time (Eq. 13)	$\delta$	Thermal thickness (m)
FHR	Flame heat release (MJ/m <sup>2</sup> )	$\varepsilon$	Emissivity (–)
GHR	Glow heat release (MJ/m <sup>2</sup> )	$\lambda$	Thermal conductivity (kW/K m)
$h$	Heat transfer coefficient (kW/K m <sup>2</sup> )	<b>Subscripts</b>	
HRR	Heat release rate (kW/m <sup>2</sup> )	a	Ambient condition
$M$	Mass (kg/m <sup>2</sup> )	c	Convective component
MLG	Mass loss from glow (kg/m <sup>2</sup> )	ch	Char component
MLR	Mass loss rate (kg/s m <sup>2</sup> )	ig	Ignition condition
MLS	Measured mass loss (kg/m <sup>2</sup> )	m	Material component
$q$	Heat flux (kW/m <sup>2</sup> )	0	Initial condition
$t$	Time (s)	s	Exposed surface condition
$T$	Temperature (K)	1	First thermal wave component
		2	Second thermal wave component

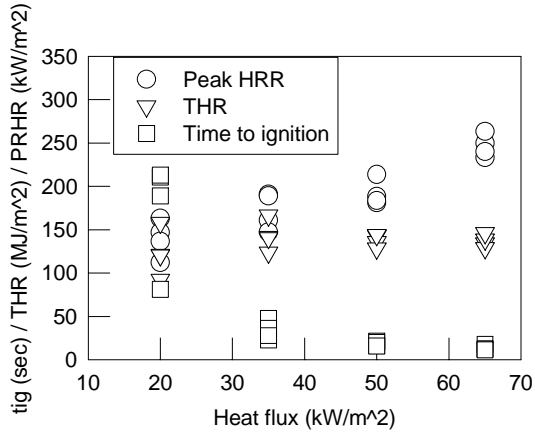


Figure 1. Cone calorimeter data for southern yellow pine.

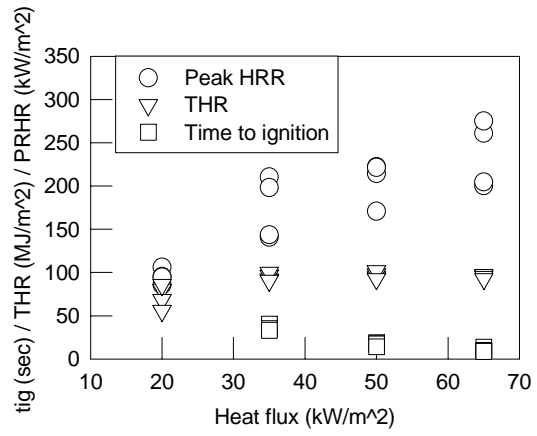


Figure 2. Cone calorimeter data for redwood.

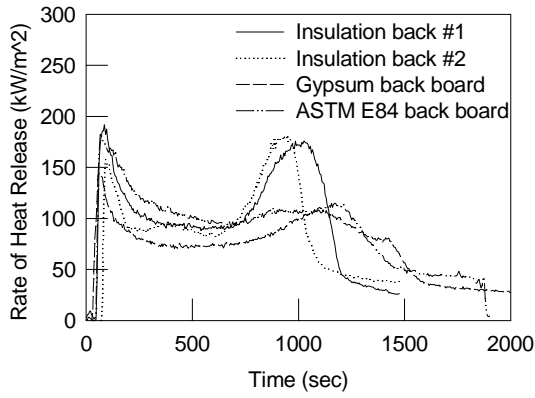


Figure 3. HRR for southern yellow pine at 35-kW/m² flux.

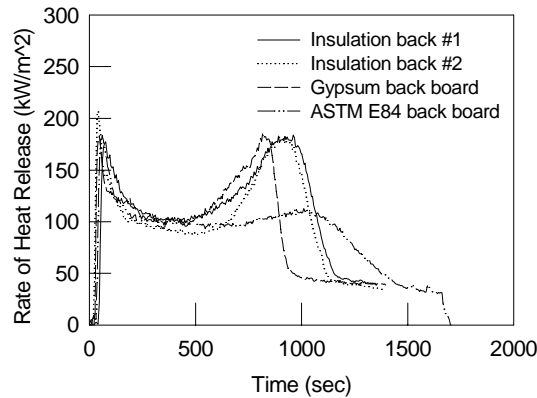


Figure 4. HRR for southern yellow pine at 50-kW/m² flux.

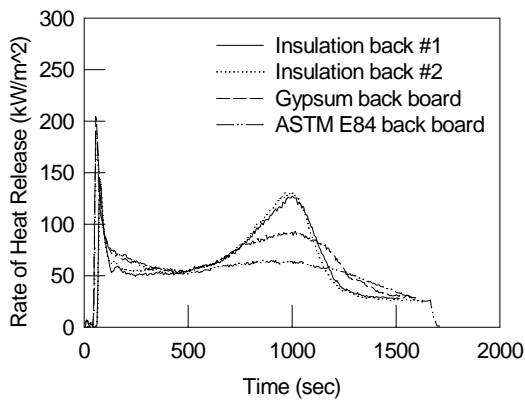


Figure 5. HRR for redwood at 35-kW/m² flux.

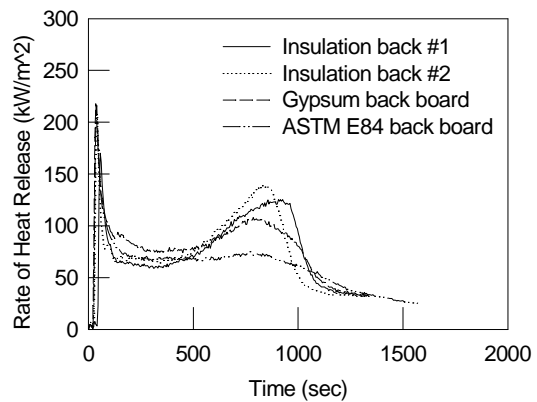


Figure 6. HRR for redwood at 50-kW/m² flux.

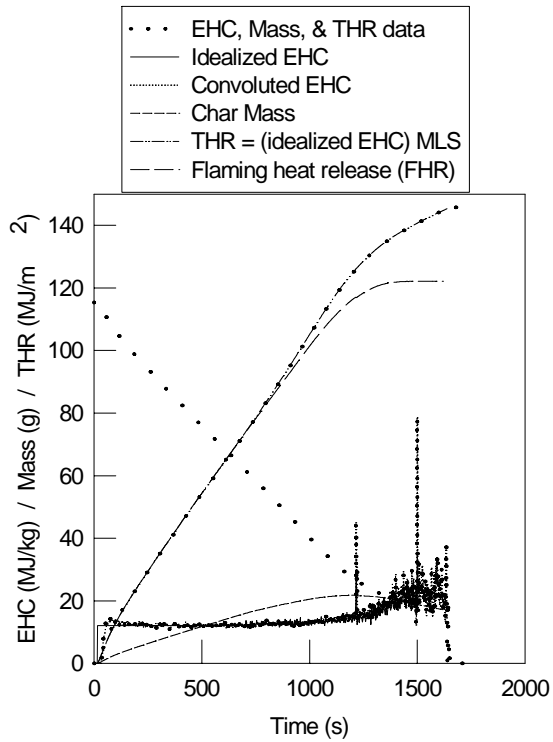


Figure 7. Combustion parameters for southern yellow pine at 50-kW/m<sup>2</sup> flux.

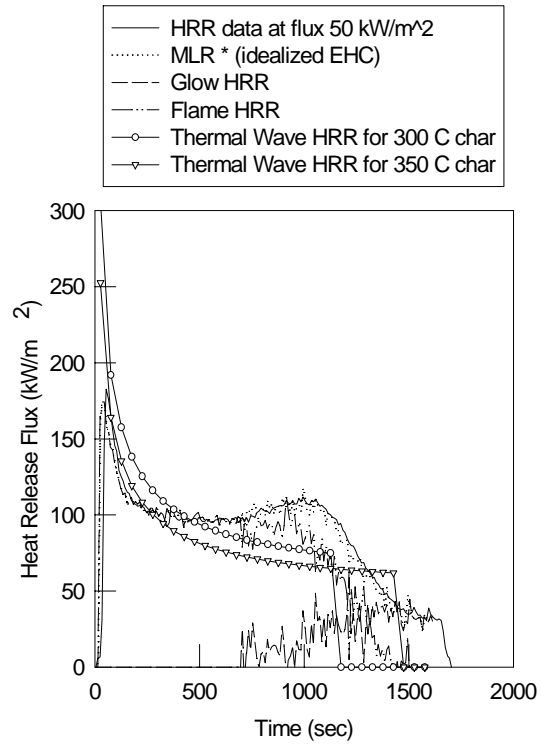


Figure 8. Reconstructed flame and glow HRR for southern yellow pine at 50-kW/m<sup>2</sup> flux.

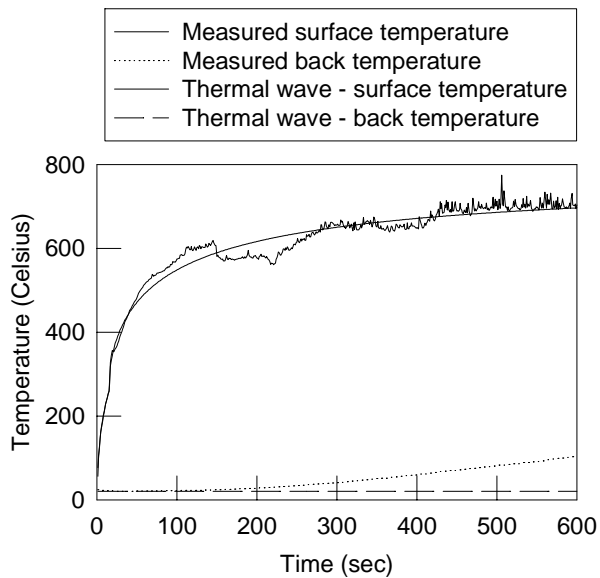


Figure 9. Thermal wave solution and thermocouple data for southern yellow pine at 50-kW/m<sup>2</sup> flux.

In: Proc. of International Conf. on Fire Safety, Columbus, OH, July 1999. Sissonville WV:  
Product Safety Corporation. Vol. 28, pp 62-73.